NUMERICAL INVESTIGATION ON COMPRESSIBLE FLOW CHARACTERISTICS IN AXIAL COMPRESSORS USING A MULTI-BLOCK FINITE-VOLUME SCHEME

B. Farhanieh, N. Amanifard and K. Ghorbanian

Department of Mechanical Engineering, Sharif University of Technology
Tehran, Iran, Bifa@sina.sharif.ac.ir - namanifard@hotmail.com - kaveh@sina.sharif.ac.ir

(Received: June 30, 2001 – Accepted in Revised From: October 13, 2001)

Abstract An unsteady two-dimensional numerical investigation was performed on the viscous flow passing through a multi-blade cascade. A Cartesian finite-volume approach was employed and it was linked to Van-Leer's and Roe's flux splitting schemes to evaluate inviscid flux terms. To prevent the oscillatory behavior of numerical results and to increase the accuracy, Monotonic Upstream Scheme for Conservation Laws (MUSCL) was added to flux splitting schemes. The Baldwin-Lomax (BL) turbulence model was implemented to solve the turbulent case studies. Implicit solution was also provided using Lower and Upper (LU) decomposition technique to compare with explicit solutions. To validate the numerical procedure, two test cases are prepared and flow over a NACA0012 airfoil was investigated and the pressure coefficients were compared to the reference data. The numerical solver was implemented to study the flow passing over a compressor cascade. The results of various combinations of splitting schemes and the MUSCL limiter were compared with each other to find the suitable methods in cascade problems. Finally, the convergence histories of implemented schemes were compared to each other to show the behavior of the solver in using various methods before implementation of them in flow instability studies.

Key Words Finite-Volume Method, Compressible Flow, Van Leer Flux Splitting, Roe Flux Splitting, High Order Limiters, Cascade Flow, Transonic Flow

چکیده مطالعه عددی دو بعدی و وابسته به زمان برای جریان حول یک زنجیره پره انجام شد تا مناسبترین روشهای عددی برای مسایل توربوماشین تعیین گردد. بر این اساس، تقریب حجم محدود به همراه روشهای شکستن شار "رو" و "ون لیر" بکار گرفته شد تا شارهای غیر لزج معادلات ناویر- استوکس محاسبه شوند. همچنین بمنظور جلوگیری از نوسانات عددی و افزایش دقت محاسبات، محدود کننده "روش بالا دست یکنواخت برای قانون محافظه کار" (MUSCL) بکار گرفته شده است. همچنین از مدل مرتبه صفر Baldwin و Lomax(BL) برای تقریب رژیم آشفته استفاده شده است و در حل ضمنی روش "تفکیک بالا و پایین" (LU) بکار گرفته شده است و با حلهای متعدد صریح مقایسه بعمل آمده است. برای ارزیابی ابزار عددی حاصل دو مورد جریان غیر لزج و لزج حول ایرفویل NACA 0012 مطالعه شده است و نتایج مطابقت خوبی با مراجع داشته است. نتایج مربوط به ترکیبهای متعدد و متنوعی از روشهای شکستن شار به همراه روشهای حل ضمنی و صریح برای جریان حول زنجیره پره، ارائه شده است که در تمامی آنها روش چند بلوکی مهمترین ترفند دستیابی به نتایج می باشد. در نهایت تاریخچه همگرایی روشهای بکارگیری متعددی در پدیده های ناپایدار معرفی گردیده‌اند.

INTRODUCTION

Historically, the analysis of the flow field in the close vicinity of the stability limit, especially in Gas-Turbine engines, has been based mainly on experimental observations and studies. Recently, several computational fluid dynamics (CFD) codes have been developed to give more powerful, low-cost design tools. The, axial compressors with their adverse pressure gradients in through flow direction, is the most critical component in Gas-Turbine engines from the viewpoint of flow instability phenomena. Several experimental observations on flow characteristics in axial compressors have been developed during recent years [1-3]. Some approximated theoretical models, derived from experimental observations are also defined. For long-length-scale disturbances introduced by Garnier et al. [4], two-dimensional linearized stability analysis were implemented by Moor et al.

[5] and Longely et al. [6].

Today, the use of CFD tools is a standard practice in the study of the cascade flow within the stable operating range of a compressor. In this regard, the CFD approach still needs to be established as a sound prediction method for operation in the unstable region.

To a lesser degree, rotating stall inception has been numerically investigated [7-8]. Nishizawa et al. [9] have studied propagating stall in isolated linear cascade using vortex methods. Outa et al. [10] have also reported on stall behavior in a two-dimensional rotor-stator system. A numerical solution for the inviscid flow in a one-stage axial compressor are presented and compared with experimental data for operation in the rotating stall region [11].

The scope of the work described in this paper was to introduce a time-marching finite volume solver for compressible multi-blades cascade flows, and to evaluate the implementation of recent finite-volume methods in turbomachinery studies. The governing equations were solved using both explicit and implicit techniques. The implicit LU decomposition was employed as the implicit solution technique [12].

GOVERNINIG EQUATIONS

For a given thermodynamic system having two intensive degree of freedom, its fluid dynamic behaviour can generally be described by means of the system of conservation laws corresponding to the conservation of total mass, momentum and energy.

Let **Q** be an unknown vector defined for a two-dimensional study as follows:

$$\mathbf{Q}=[\rho, \rho u, \rho v, \rho E]^T = [q_1, q_2, q_3, q_4]^T \quad (1)$$

Where E is the total energy ($E = e + (u^2 + v^2)/2$). Let V be any volume with bounding surface ∂V and outward unit normal **n**. Assuming that the volume does not vary with time, **Q** satisfies the following integral conservation law:

$$\frac{d}{dt}\int_V \mathbf{Q}\, dV = \int_V \frac{\partial}{\partial t}\mathbf{Q} dV = -\oint_{\partial V} \mathbf{F} \cdot \mathbf{n}\, dS \quad (2)$$

The equivalent differential form of Equation 2 in an inertial reference system reads:

$$\frac{\partial}{\partial t}\mathbf{Q} = -\nabla \cdot \mathbf{F} \quad (3)$$

This accounts for the inviscid ($\mathbf{F}_E$) and viscous ($\mathbf{F}_V$) contributions, i.e.

$$\mathbf{F} = \mathbf{F}_E - \mathbf{F}_V \quad (4)$$

Where

$$\mathbf{F}_E = [\rho \mathbf{u},\ \rho \mathbf{uu} + p\mathbf{I},\ \rho \mathbf{u}H]^T \quad (5\text{-a})$$

$$\mathbf{F}_V = [0,\ \sigma,\ -(\mathbf{q} - \mathbf{u} \cdot \sigma)]^T \quad (5\text{-b})$$

and

$$\sigma = \mu(\nabla \mathbf{u} + \nabla \mathbf{u}^T) - \frac{2}{3}\mu \nabla \cdot \mathbf{uI} \quad (6)$$

$$\mathbf{q} = -\lambda \nabla T \quad (7)$$

The governing equations are transformed to a computaional space for the numerical solution. Hence, they are as following:

$$\frac{\partial \overline{\mathbf{Q}}}{\partial \tau} + \frac{\partial \overline{\mathbf{E}}}{\partial \xi} + \frac{\partial \overline{\mathbf{F}}}{\partial \eta} = \frac{\partial \overline{\mathbf{E}}_v}{\partial \xi} + \frac{\partial \overline{\mathbf{F}}_v}{\partial \eta} \quad (8)$$

In which, $\overline{\mathbf{Q}}$ is the unknown vector, $\overline{\mathbf{E}}$, and $\overline{\mathbf{F}}$ are the inviscid flux vectors in ξ and η direction respectively. $\overline{\mathbf{E}}_v$ is the vicous flux vector in ξ direction, and $\overline{\mathbf{F}}_v$ is the viscous flux vector in η direction. They are related to physical vectors with the following general relations:

$$\overline{\mathbf{Q}} = \frac{\mathbf{Q}}{J} \quad (9\text{-a})$$

$$\overline{\mathbf{E}} = \frac{1}{J}(\xi_x \mathbf{F}_{Ex} + \xi_y \mathbf{F}_{Ey}) \quad (9\text{-b})$$

$$\overline{\mathbf{F}} = \frac{1}{J}(\eta_x \mathbf{F}_{Ex} + \eta_y \mathbf{F}_{Ey}) \quad (9\text{-c})$$

$$\overline{\mathbf{E}_v} = \frac{1}{J}(\xi_x \mathbf{F}_{vx} + \xi_y \mathbf{F}_{vy}) \quad (9\text{-d})$$

$$\overline{\mathbf{F}_v} = \frac{1}{J}(\eta_x \mathbf{F}_{vx} + \eta_y \mathbf{F}_{vy}) \quad (9\text{-e})$$

where

$$J=\frac{1}{x_\xi y_\eta - y_\xi x_\eta}=\frac{\partial(\xi,\eta)}{\partial(x,y)} \tag{10}$$

Regarding to two-dimensional approach in present work, the governing equations for relative frame is the same as those in absolute frame, because there is no Coriolis acceleration (no radial component of velocity). Consequently, the only treatment in stationary-cascade studies (if desired) is the using of absolute velocities in place of relative velocities in solver. As evident, the absolute velocities are achieved by adding the rotation speed to relative velocities, computed in rotating frame.

NUMERICAL PROCEDURE

Finite Volume Formulation Reconsidering Equation 8, the time derivative is approximated by a first-order backward differencing quotient and the remaining terms are evaluated at time level n+1. Thus:

$$\frac{\overline{\mathbf{Q}}^{n+1}-\overline{\mathbf{Q}}^{n}}{\Delta\tau}+\left(\frac{\partial\overline{\mathbf{E}}}{\partial\xi}\right)^{n+1}+\left(\frac{\partial\overline{\mathbf{F}}}{\partial\eta}\right)^{n+1} =\left(\frac{\partial\overline{\mathbf{E}}_v}{\partial\xi}\right)^{n+1}+\left(\frac{\partial\overline{\mathbf{F}}_v}{\partial\eta}\right)^{n+1} \tag{11}$$

Integrating Equation 11 over square **ABCD** shown in Figure 1, and using Green's theorem provides:

$$\Delta\overline{\mathbf{Q}}+\frac{\Delta\tau}{\Delta\xi}(\overline{\mathbf{E}}_r-\overline{\mathbf{E}}_l)+\frac{\Delta\tau}{\Delta\eta}(\overline{\mathbf{F}}_t-\overline{\mathbf{F}}_b)= \frac{\Delta\tau}{\Delta\xi}(\overline{\mathbf{E}}_{vr}-\overline{\mathbf{E}}_{vl})+\frac{\Delta\tau}{\Delta\eta}(\overline{\mathbf{F}}_{vt}-\overline{\mathbf{F}}_{vb}) \tag{12}$$

Since, in Eq. 12, the flux vectors are evaluated in time step n+1; they can be expressed in terms of $\Delta\overline{\mathbf{Q}}$. By using the Taylor expansion and a first order approximation in time, the fux vectors are evaluated as follows:

$$\overline{\mathbf{E}}^{n+1}=\overline{\mathbf{E}}^{n}+\frac{\partial\overline{\mathbf{E}}}{\partial\overline{\mathbf{Q}}}\Delta\overline{\mathbf{Q}}=\overline{\mathbf{E}}^{n}+\mathbf{A}\Delta\overline{\mathbf{Q}} \tag{13-a}$$

$$\overline{\mathbf{F}}^{n+1}=\overline{\mathbf{F}}^{n}+\frac{\partial\overline{\mathbf{F}}}{\partial\overline{\mathbf{Q}}}\Delta\overline{\mathbf{Q}}=\overline{\mathbf{F}}^{n}+\mathbf{B}\Delta\overline{\mathbf{Q}} \tag{13-b}$$

$$\overline{\mathbf{E}}_v^{n+1}=\overline{\mathbf{E}}_v^{n}+\frac{\partial\overline{\mathbf{E}}_v}{\partial\overline{\mathbf{Q}}}\Delta\overline{\mathbf{Q}}=\overline{\mathbf{E}}_v^{n}+\mathbf{A}_v\Delta\overline{\mathbf{Q}} \tag{13-c}$$

$$\overline{\mathbf{F}}_v^{n+1}=\overline{\mathbf{F}}_v^{n}+\frac{\partial\overline{\mathbf{F}}_v}{\partial\overline{\mathbf{Q}}}\Delta\overline{\mathbf{Q}}=\overline{\mathbf{F}}_v^{n}+\mathbf{B}_v\Delta\overline{\mathbf{Q}} \tag{13-d}$$

The matrices A, B, A_v, and B_v are the Jacobian matrices given by Hoffman et al. [12].

Since, evaluation of inviscid flux vectors on cell faces is the most important problem in numerical solution of Euler and N-S equations, the flux splitting methods are discussed in details in the following section. The second-order derivatives are evaluated by central difference approximation, because these terms may not cause oscillations in computational domain [12].

Flux Vector Splitting To avoid the addition of artificial viscosity, the flux vector splitting schemes used to formulate the convective terms.

For a system of hyperbolic equations, the Jacobian matrix **A** must possess real eigenvalues. The eigenvalues of **A** represents the charactristic direction of the hyperbolic system and thus provide the direction of the propagation of information. If

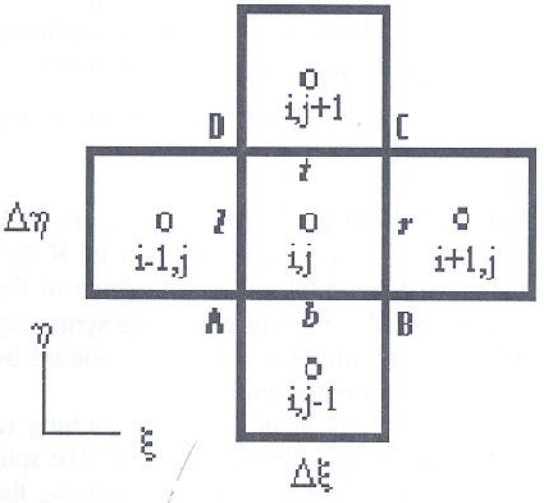

Figure 1. Definition of a Cartesian finite-volume cell.

matrix $\mathbf{A}$ has real eigenvalues and associated eigenvectors, it may be diagonalized; i.e., a similarity transformation exists such that:

$$\mathbf{A} = \mathbf{L}^{-1}\Lambda_g \mathbf{L} \tag{14}$$

For a Jacobian matrix like $\mathbf{A}$, a large class of flux decomposition can be obtained by defining $\mathbf{A}^{\pm}$ as follows:

$$\mathbf{A}^{\pm} = \frac{\mathbf{A} \pm g(\mathbf{A})}{2} \tag{15}$$

and

$$\overline{\mathbf{E}}^{\pm} = \mathbf{A}^{\pm}\overline{\mathbf{Q}} \tag{16}$$

where g(**A**) is:

$$g(\mathbf{A}) = \mathbf{L}^{-1}\Lambda_g \mathbf{L} \tag{17}$$

and Λ_g is a diagonal matrix whose non-zero coefficients are g_i.

Following the current definition, the numerical flux function associated with a flux vector splitting is expressed as:

$$\overline{\mathbf{E}}_r = \overline{\mathbf{E}}^{+}(\overline{\mathbf{Q}}_{i,j}) + \overline{\mathbf{E}}^{-}(\overline{\mathbf{Q}}_{i+1,j}) \tag{18}$$

Similar functions can be defined for other flux vectors at all faces of the finite volume cell.

Two more advanced flux vector-splitting methods are implemented in present study to evaluate $\overline{\mathbf{E}}^{\pm}$. They are briefly discussed in the following section.

Van Leer's splitting In this method, the split fluxes are represented by a polynomial in M that gives the same functional values and slope of the unsplit fluxes at $M = \pm 1$. Moreover, the symmetry properties of each split flux component should be the same as those of the unsplit one .

An extension of the Van Leer-type splitting to multidimensional flows is not quite trivial. The split flux component can be constructed by retaining the one-dimensional structure. The method conditions, and the matrix form of split flux vectors for two dimentional studies in computational space is reported by Hoffman [12].

Approximate Riemann solver (Roe splitting) The idea of Roe consist of determining the solution by solving a modified equation, where the flux $\overline{\mathbf{E}}$ is quasilinearized by introducing a matrix $\tilde{\mathbf{A}}$ and adopting $\overline{\mathbf{E}} = \tilde{\mathbf{A}}\,\overline{\mathbf{Q}}$.

Assuming that the discretized solution of the system of conservation laws is piecewise constant within each computational volume, the solution of one-dimensional non-linear equation is equivalent to solving approximately a Riemann-type problem at cell interfaces. The total averaged flux function at each cell, and the properties required for Roe flux splitting method are reported by peyret et. al.[13].

Construction of high-order methods High-order methods can be constructed in many ways. Total Variation Diminishing (TVD), and the Monotonic Upstream Schemes for Conservation Laws (MUSCL) are the most famous methods related to the design of high-order schemes[13].

According to Van Leer's point of view, upwind methods can be interpreted as a projection phase followed by an evolution phase. In the projection (or reconstruction) phase the piecewise continuous initial values are interpolated to yield a continuous distribution within each computational cell, while the evolution phase corresponds to the updating of averaged unknown variable $\hat{u}$ exploiting the reconstructed solution.

In this work the MUSCL limiter is used due to its high accuracy.

For an unknown variable u the MUSCL can be expressed as[13]:

$$u_l^n = u_i^n + \frac{1}{4}[(1-r)\bar{\delta}^{+}u_{i-1}^n + (1+r)\hat{\delta}^{+}u_i^n] \tag{19}$$

$$u_r^n = u_{i+1}^n - \frac{1}{4}[(1-r)\bar{\delta}^{+}u_{i+1}^n + (1+r)\hat{\delta}^{+}u_i^n] \tag{20}$$

A set of limiters are defined in Table 1 upon values of r And $\hat{\delta}^{+}, \bar{\delta}^{+}$ are the limited slopes:

$$\hat{\delta}^{+}u = \ell(\delta^{+}u_i, \omega\delta^{+}u_{i-1})\ ;\ \bar{\delta}^{+}u = \ell(\delta^{+}u_i, \omega\delta^{+}u_{i+1}) \tag{21}$$

TABLE 1. Definition of Limiters Upon Values of r.

r	Name of Limiter
1/3	Third-order upwind biased scheme
1	Three-point central difference scheme
-1	Fully upwind scheme
0	Fromm scheme

where $1 \le \omega \ge (3-r)/(1-r)$, and ℓ is a limiter function such as, Van Leer and Roe's minmod limiter functions. The simplified form of MUSCL using Van Leer's function becomes[13]:

$$\ell = \frac{2\delta^- u.\delta^+ u}{[(\delta^- u)^2 + (\delta^+ u)^2]}$$
$$f = (1 - r\cdot\ell)\delta^- u + (1 + r\cdot\ell)\delta^+ u \qquad (22)$$
$$u_r = u_{i+1,j} - \frac{1}{4} f\cdot\ell$$

Stability Criteria To overcome the solution instabilities in explicit techniques, MacCormack stability criteria is employed to obtain the appropriate time step [12]:

$$\Delta\tau \le \frac{S_f(\Delta\tau)_{inv}}{1 + 2/\mathrm{Re}_c} \qquad (23)$$

in which:

$$(\Delta\tau)_{inv} \le \left\{ \frac{1}{\frac{|U|}{\Delta\xi} + \frac{|V|}{\Delta\eta} + a\left[\frac{1}{(\Delta\xi)^2} + \frac{1}{(\Delta\eta)^2}\right]} \right\} \qquad (24)$$

and Re_c is:

$$\mathrm{Re}_c = \min(\mathrm{Re}_\xi, \mathrm{Re}_\eta) \qquad (25)$$

Also U and V are the contravariant velocity components and the cell Reynolds numbers are defined as following:

$$\mathrm{Re}_\xi = \frac{\rho|U|\Delta\xi}{\mu} \qquad (26)$$

$$\mathrm{Re}_\eta = \frac{\rho|V|\Delta\eta}{\mu} \qquad (27)$$

NUMERICAL BOUNDARY CONDITIONS

Inflow and Outflow Boundary Conditions All inflow and outflow boundary conditions are prescribed based on the sign of the eigenvalues. These eigenvalues indicate how information is propagated at the boundaries.

Our inflow is subsonic, so three of the four eigenvalues are positive, i. e., coming from outside, and one is negative, i. e., coming from inside. Therefore, three analytical boundary conditions should be specified from outside and the other determined from inside.

If the outflow is subsonic, three of the four eigenvalues are positive, i. e., outgoing, and one is negative, i. e., and incoming from the outside. Therefore, one analytical boundary condition may be specified; and the others are determined from the computational domain by extrapolation.

The triple variables from outside at the inlet can be selected in the following ways:

1. Selecting P_t, T_t and inflow angle.
2. Selecting T_s , u and v.
3. Selecting P_s, u and v.

For subsonic outflow boundary conditions, P_s is fixed.

Figure 2 illustrates a schematic shape of computational domain and the hatched cells are the fictitious boundary cells which contains the boundary values.

Solid Wall Boundary Condition For no slip wall condition, the velocities at both sides of the wall are given opposite in sign in order to cancel out each other.

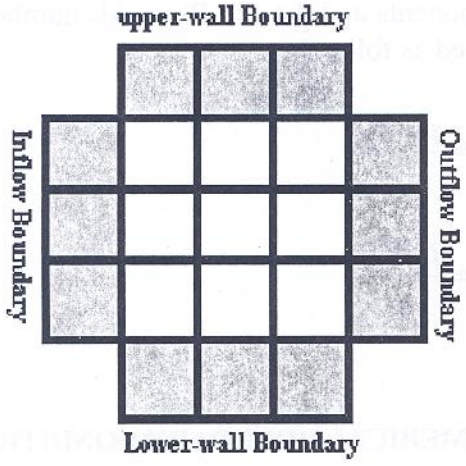

Figure 2. Schemenc shape of computational domain.

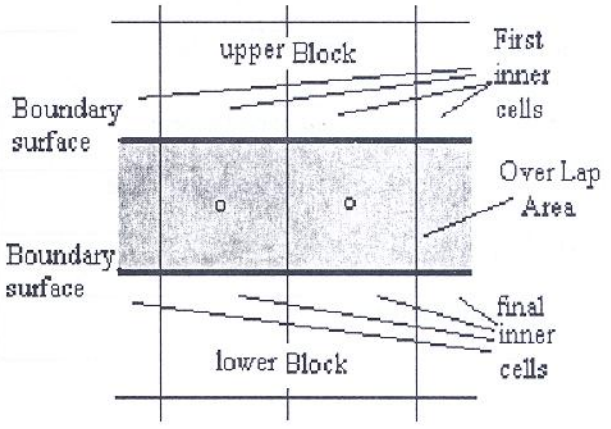

Figure 3. Schematic shape of block boundary condition.

Initial Guess Due to the hyperbolic-parabolic nature of the N-S equations in time marching methods, only one set of initial condition is required. Pressure and temperature are set equal to total thermodynamics conditions of inflow and the velocity components are set equal to zero.

The Neighborhood Block Boundary Condition Each block shares one or more boundaries with its surrounding blocks. The exchange of data among the blocks takes place through their common boundaries. The mechanism of implementing above-mentioned boundary condition is described in the following section.

The Multi-Blocks Algorithm In each time step, the solver sweeps all cells from first to final block in turn. In this regard, cell index is defined as follows:

$$ind(i,j) = i + [(iblock-1)jmax-(j-1)]imax \qquad (28)$$

Figure 3 shows a schematic shape of computational domain near the common boundary of two adjacent blocks.

In the common boundary, there is an overlap area, in which fictitious cells of upper and lower blocks cover each other. These cells do not exist physically and they are just the temporary cells to save boundary data. The map of physical surface in multi-block computational space, named 'Boundary surface', is shown in Figure 3 by thick-solid lines. It is obvious that there must be two maps for a physical surface for two mapped blocks.

Grid Generation Each passage (between two blades) has an individual mesh, which is generated by mesh generator program using PDE method. Clustering is available by related source terms as well as orthogonality. The mesh generated for each individual passage is considered as a single block, and the multi-blocks algorithm assembles them to prepare the complete area of solution.

Turbulence Model One of the groups of statistical turbulence models is the algebraic one or two-layer turbulence closure. These models can easily be implemented into a numerical algorithm, but they require the determination of boundary layer parameters to calculate the eddy viscosity. In complex flow such as the flow through a turbine or compressor cascade, the calculation of e.g. shear layer thickness in a CFD code is difficult, because no realistic criterion can be used to define the edge of the boundary layer [14]. That is specially the case when flow separation exists within the domain.

A algebraic model, which is not written in terms of the boundary layer quantities and is very robust in separated regions is the modified Baldwin-Lomax (BL) model [15]. The BL model is implemented by [16] in numerical investigation of Rotating-Stall inception in a multi-blade cascade flow in an axial compressor, which the flow may have large scale separated zones. Moreover, the comparison of other turbulence models such as κ-ε with BL model in [14] shows the adequate assurance

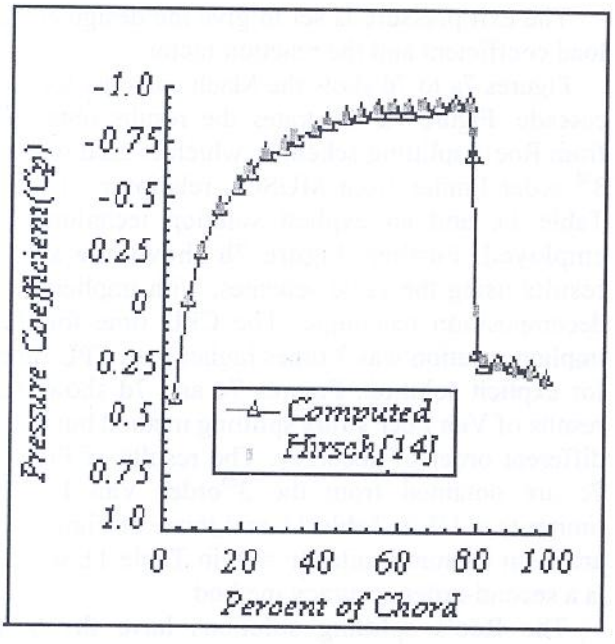

Figure 4. Comparing computed and reference curves of pressure coefficient (Cp) for airfoil of NACA0012.

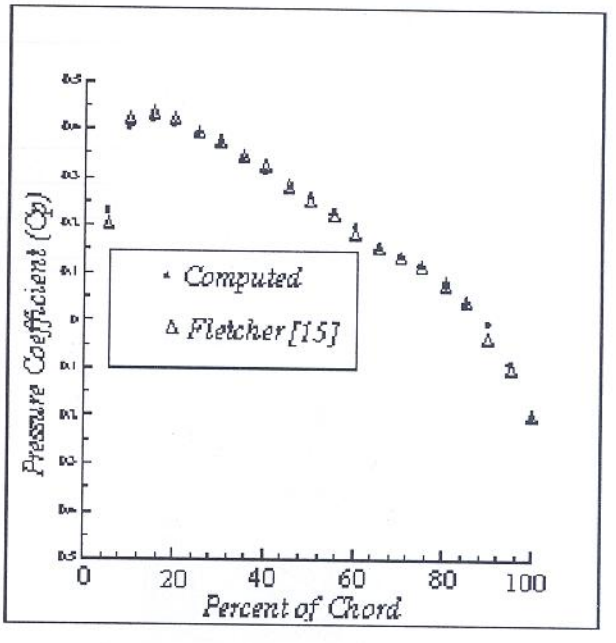

Figure 5. Comparing computed and experimental results for flow over a NACA0012 airfoil at M= 0.4 and Re= 10^6.

of using BL model in cascade problems. Regarding a large amount memory required in multi-blades studies, the BL consumes the least memory and CPU time with respect to higher-order turbulence models. Consequently, for present work the BL model is preferred.

DISCUSSION OF RESULTS

Code Validation Comparing the computed results to other approved dada's assesses the performance of the described methodology.

The first validation test case is prepared for inviscid flow over half of the NACA0012 airfoil. In Figure 4, the pressure coefficient (Cp) distribution was compared with [17]. The flow is transonic, the inlet Mach number is equal to 0.85, and the angle of attack is zero. The computed results are in good agreement with the reference data. This test case is prepared to validate the solution of inviscid terms and the related implemented techniques.

The second prepared test case is the subsonic viscous flow around NACA0012 airfoil. The Reynolds number is set to 10^6 and the flow is turbulent. The inlet Mach number is set to 0.4, to test the density-based solver in lower Mach numbers. The angle of attack is zero. The transition point is set near the leading edge (proposed in [18]). The computed results are in good agreement with experimental results reported in [19]. This test case is prepared to validate the solver in viscous – turbulent flows, which is a very usual condition in flows, through compressor cascades.

Cascade Results In the third test case, the transonic flow through a multi-block passage (cascade) problem was solved and the results are illustrated in Figures 6a and 6b. The airfoil geometry chosen for this problem is the same as the geometry used by Saxer et.al. [11], for a cascade of an axial compressor.

In this test case, a rotor cascade was studied in design condition to investigate the implementation of various methods in complicated areas. The design conditions are given in Table 2. The velocity vectors are computed in relative frame.

All the computations are done for mean radius. The compressor is a transonic multi-stage type and the flow is viscous and turbulent (the Reynolds number based on chord is 10^6).

TABLE 2. The Design Condition Parameters.

r_h/r_t	0.6
R	0.45
P_{in}	101325 Pa
T_{in}	300°K

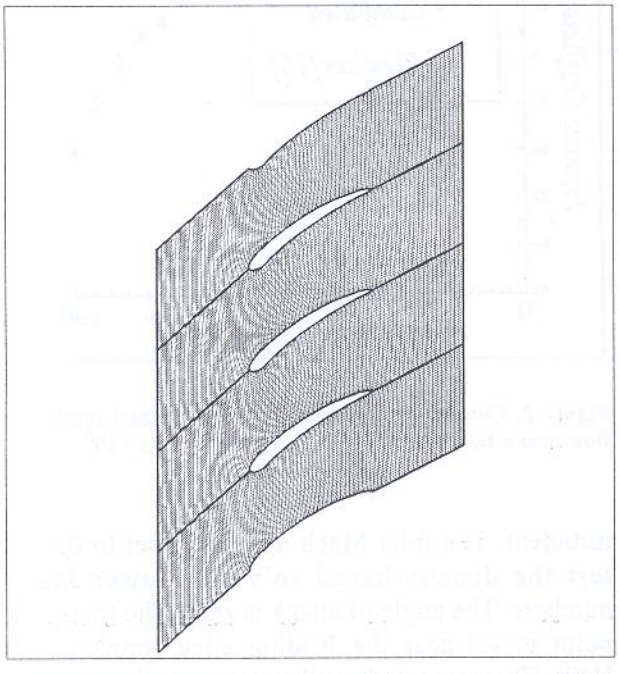

Figure 6a. Mesh generated for a 3-blade cascade (a 76×41 grid is used for each passage).

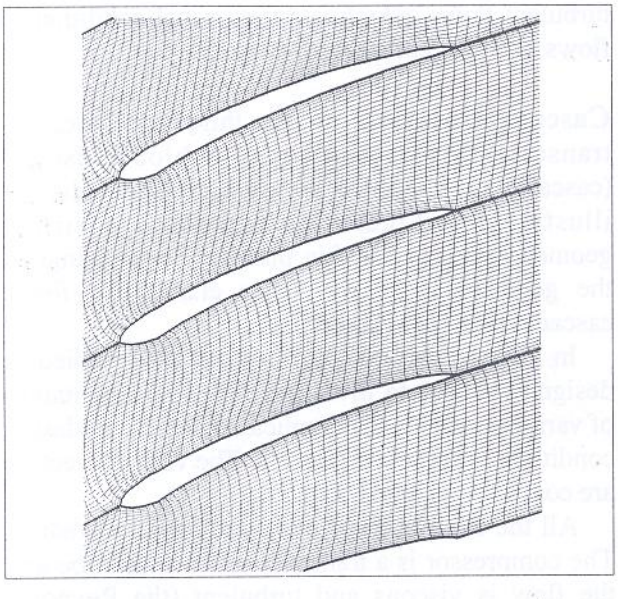

Figure 6b. Zoomed image of mesh generated for a 3-blade cascade (a 76×41 grid is used for each passage).

The exit pressure is set to give the design stage load coefficient and the reaction factor.

Figures 7a to 7d show the Mach contours for the cascade. Figure 7a illustrates the results obtained from Roe's splitting schemes, which is used with a 3rd order limiter from MUSCL relation(r =1/3 in Table 1), and an explicit solution technique is employed. Further, Figure 7b shows the same results using the same schemes, with implicit LU decomposition technique. The CPU time for the implicit solution was 3 times higher than CPU time for explicit solution. Figures 7c and 7d show the results of Van Leer's flux splitting method but with different order of accuracy. The results of Figure 7c are obtained from the 3rdorder Van Leer's limiter (r = 1/3 in Table 1), and those of Figure 7d are from Fromm limiter (r = 0, in Table 1), which is a second-order accuracy method.

The Roe's splitting solutions have the best accuracy but consumes higher CPU time compared with Van Leer's splitting solutions (approximately 1.3 times). The results shown in Figures 7a to 7d are similar, and show good agreements with each other in their range of the Mach number. The velocity vectors, streamlines, pressure contours, temperature contours are plotted and presented in Figures 8 to 11 respectively. The Van Leer's splitting and the 3rdorder limiter is used for obtaining the results shown in Figures 8 to 11. In Figure 10, oblique shocks have been captured near the leading edge of airfoils that shows the shock-capturing characteristic of the solver. In Figure 11, the majority of high-pressure gradients are accumulated near the lower left corner of the first block. This phenomenon is due to the solid wall effect of lower boundary of the cascade. Therefore, an impact-type phenomenon takes place when the flow impinges into the leading edge of the curved part of lower boundary (The angle of lower wall is higher than flow inlet angle). The solid wall condition in lower and upper wall is set to give the similar condition of a cascade wind tunnel. The wall effect shown in Figure 11 is a very common effect in experimental cascade studies. As evident, using the periodic boundary condition in computations, for lower and upper walls of the cascade removes the wall effects. Figure 12 provides a comparison between various methods used in the present work. The convergence histories of implemented methods are compared to

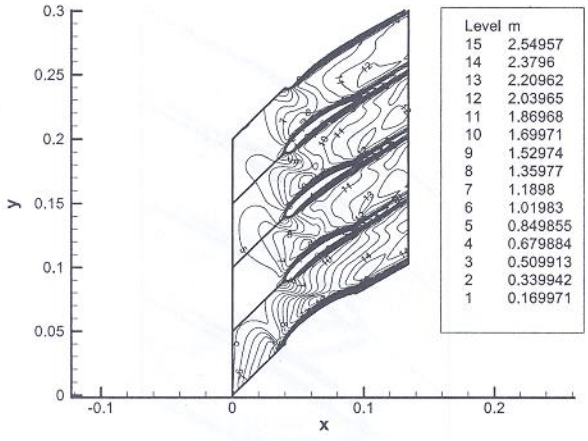

Figure 7a. Mach contours for a 3-blade cascade, using Roe's splitting scheme with 3rd order Van Leer's universal limiter and explicit solution (Range of contours: 0.2-2.55).

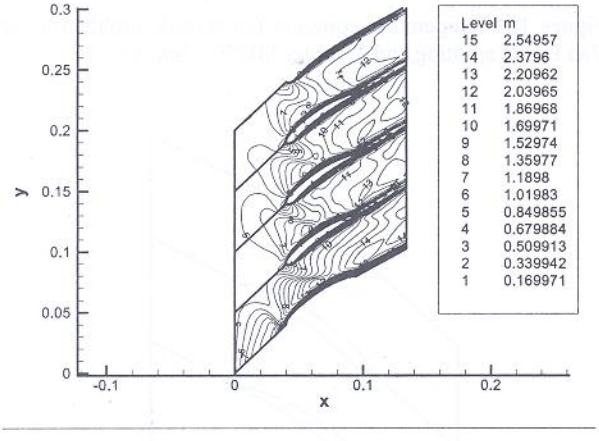

Figure 7b. Mach contours for a 3-blade cascade, using Roe's splitting scheme with 3rd order MUSCL limiter and implicit solution (Range of contours: 0.2-2.55).

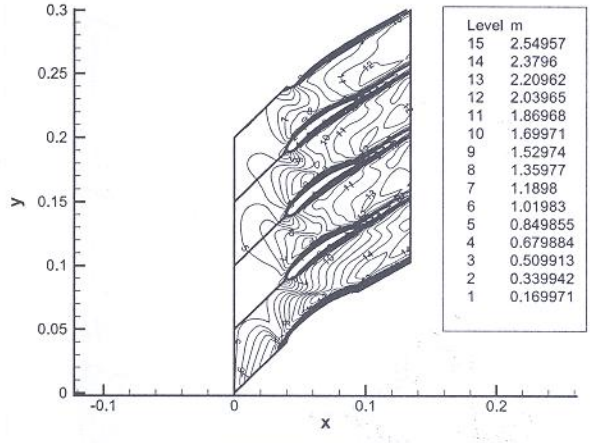

Figure 7c. Mach contours for a 3-blade cascade, using Van Leer's splitting scheme with 3rd order MUSCL limiter and explicit solution (Range of contours: 0.083-2.5472).

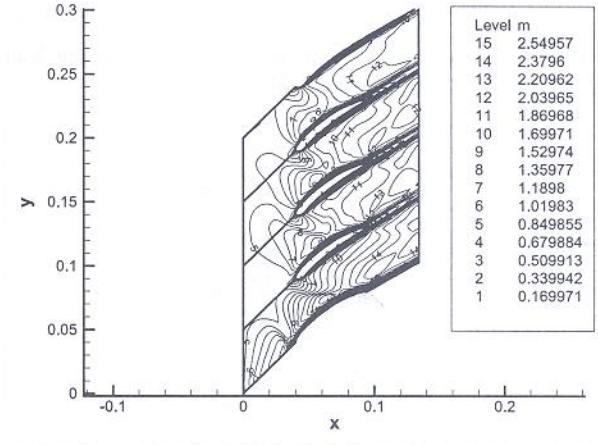

Figure 7d. Mach contours for a 3-blade cascade, using Roe's splitting scheme with Fromm limiter, obtained from MUSCL relation, and explicit solution. (Range of contours: 0.2-2.55).

each other in a 5000 iteration range. The vertical axis of Figure 12 is the logarithm of normalized relative-error of ρ(density), averaged over the computational domain. The results show a higher accuracy of Roe's splitting algorithm and the less accuracy of implicit solution technique, during the first 5000 iterations. However, the implicit methods may cause later convergence but the same accuracy for higher iterations. Using implicit techniques increases the cost of computations in reported range of iterations.

It is also seen that the difference between Van Leer's splitting errors and those of Roe's are relatively small (they have the same order of accuracy). The mentioned error for each cell, using explicit techniques reaches a minimum of 10^{-8}, whereas for implicit solution this error reaches a minimum of 10^{-7} in the 5000 iterations.

CONCLUSION

A multi-blocks 2-D compressible solver was developed to investigate the performance of numerical schemes in turbomachinery through-flow problems that may need enormous amounts of grid cells and

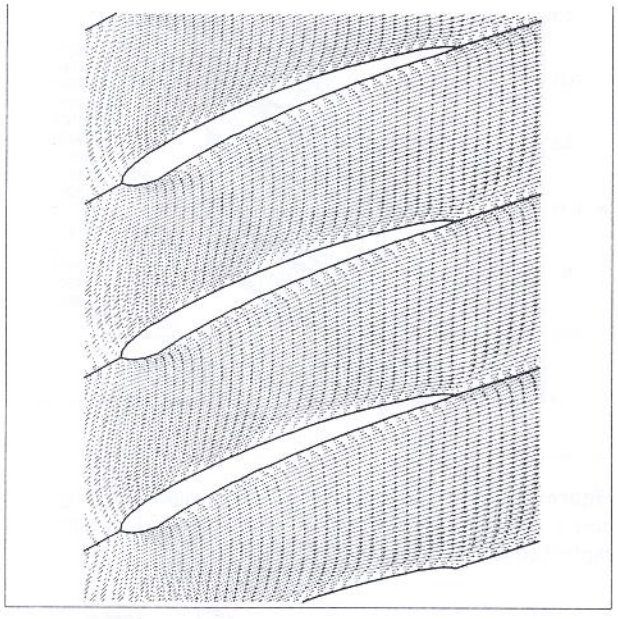

Figure 8. Velocity vectors for cascade problem using Van Leer's splitting and 3rd order MUSCL limiter.

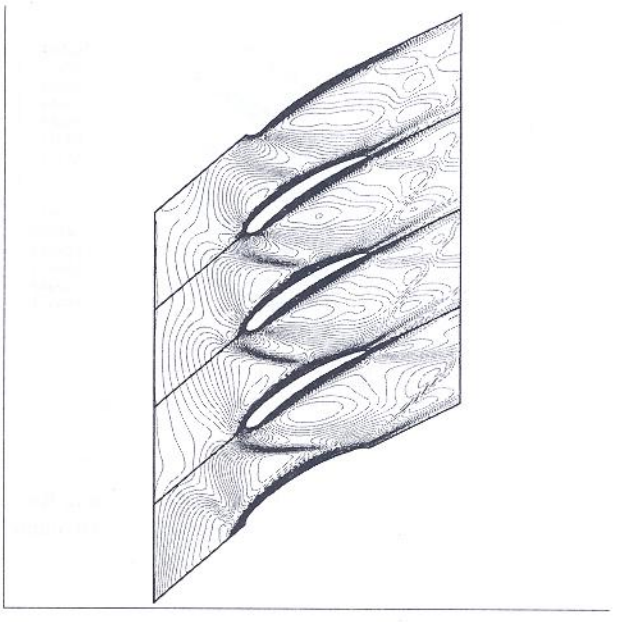

Figure 10. Temperature contours for cascade problem using Van Leer's splitting and 3rd order MUSCL limiter.

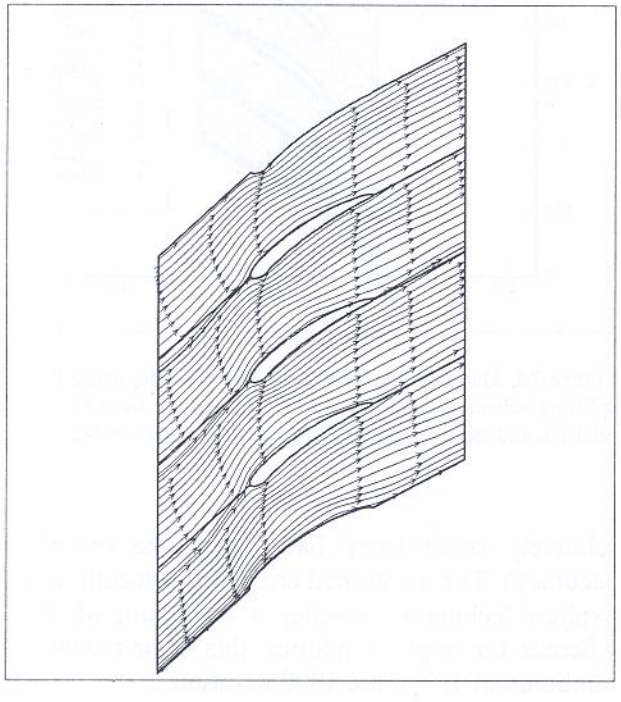

Figure 9. Streamlines for cascade problem using Van Leer's splitting and 3rd order MUSCL limiter.

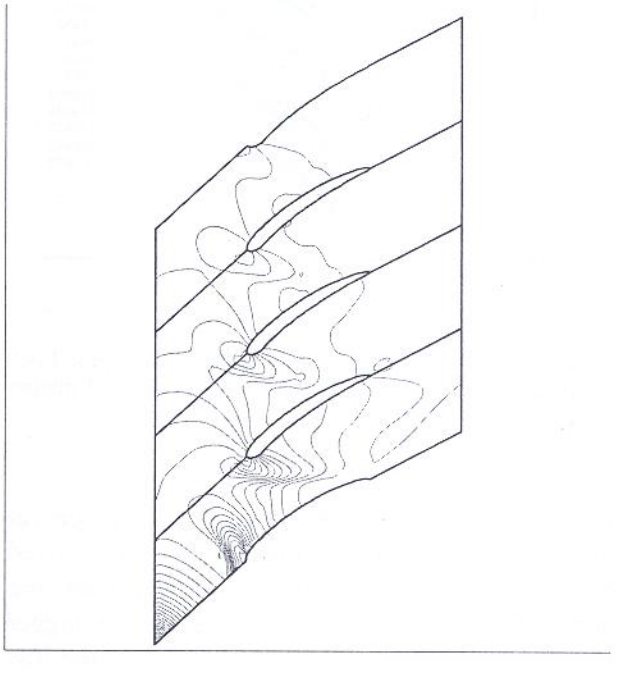

Figure 11. Pressure contours for cascade problem using Van Leer's splitting and 3rd order MUSCL limiter.

CPU times. Inviscid flow around an airfoil NACA0012 was observed to show the required assurance of the solver in its inviscid part of solution. Further, the viscous-turbulent flow around the same airfoil was observed, to validate the solver in a viscous flow. The test cases of NACA0012 airfoil gave the required assurance about the solver.

To use the solver for investigation of flow instabilities in multi-blade cascades and to study

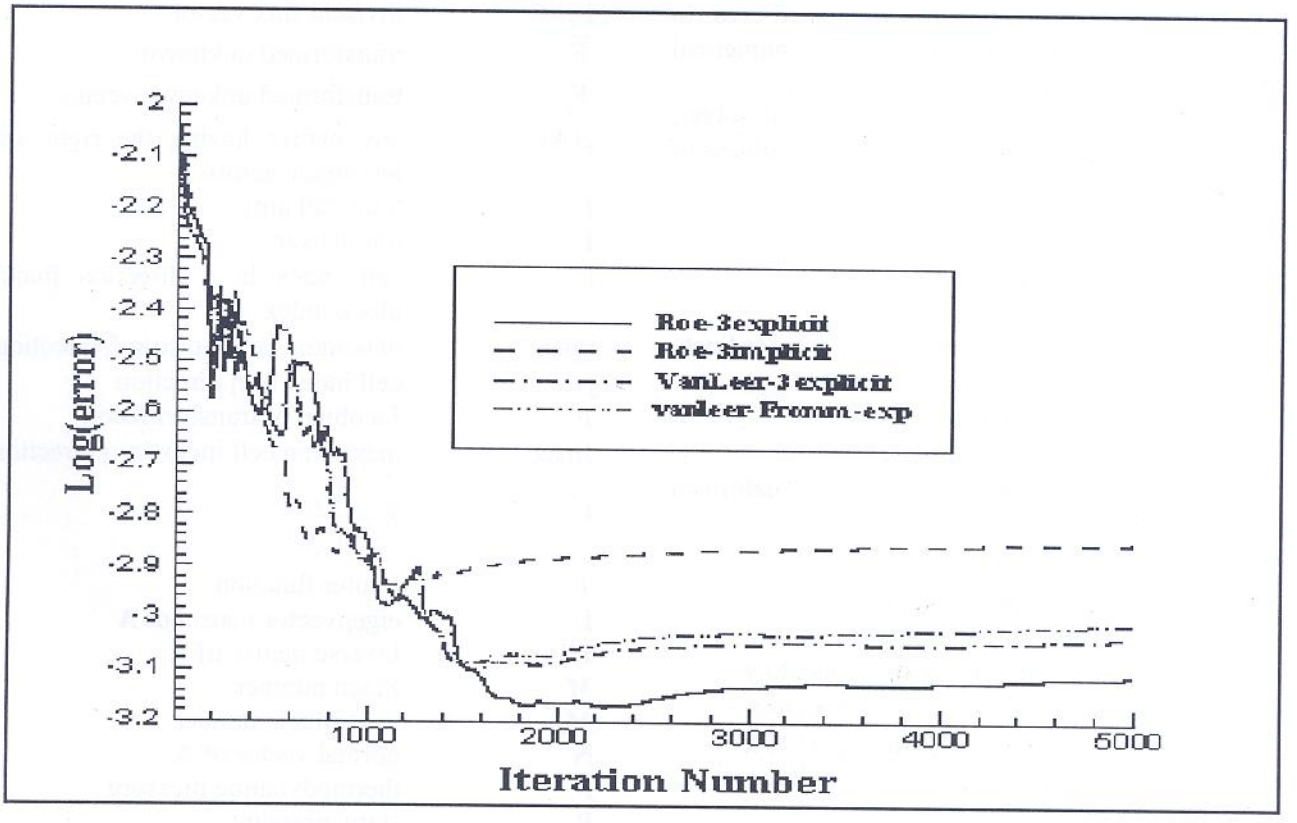

Figure 12. Comparison of convergence histories of various methods. The vertical axis shows the logarithm of normalized averaged error in the entire computational domain and the horizontal axis shows the number of time steps.

unsteady phenomena, like Rotating-stall in axial compressors, a third test case was prepared. The viscous-turbulent flow in a 3-blade cascade of an axial compressor was studied, in a sample design condition of the compressor stage.

Two different flux vector-splitting schemes with MUSCL limiter were implemented. Implicit and explicit techniques were both employed and their results were compared with each other. The convergence history during 5000 iterations shown that the explicit solver was faster than the implicit one to reach the first minimum amplitude of the error, and the implicit technique had the lower accuracy during the mentioned iteration range.

The 3rd order MUSCL had the most accurate results with Van Leer and Roe's flux splitting schemes. The Roe method consumed more CPU times but gave the most accurate results for the mentioned iteration range.

The comparison of various methods in unsteady range of solution illustrated the behavior of the solver when using various methods and techniques, which is a very important sequence before the implementation of numerical schemes in instability problems. To use the lower cost, and fast responding methods, the above-mentioned comparison was made.

The results of the Van Leer and Roe schemes had the same order of accuracy but the results of the Roe scheme had a lower bound of errors in the same order of accuracy. Both splitting schemes with a 3rd order MUSCL limiter seems to be efficient for the cascade problems in an unsteady compressible state. The implemented grid resolution for the viscous flows appears to be adequate and prevents exceeded computational efforts.

As a final conclusion, a CFD tool was introduced and several known methods were studied and

compared to each other in a complicated area, to find the suitable schemes before any numerical investigation of instability conditions.

However, future studies by the present solver, about instability effects can show the usefulness of the present work.

NOMENCLATURE

τ	time in transformed coordinate time step
σ	stress tensor
ω	slope averaging parameter
ξ	horizontal axis of transformed coordinate
ρ	density
μ	absolute viscosity
ξ_y	partial of ξ with respect to y
η_y	partial of η with respect to y
ξ_x	partial of ξ with respect to x
η_x	partial of η with respect to x
∂V	bounding surface of volume
$\lambda_I^{\pm}$	eigenvalues of $\mathbf{A}^{\pm}$
λ_I	eigenvalues of **A**
Λ_g	diagonal matrix with its elements being the eigenvalues
β_2	outlet angle of relative velocity
β_1	inlet angle of relative velocity
$\Delta\tau_{inv}$	maximum allowable
$\Delta\tau$	maximum allowable time step
ψ	load coefficient
ϕ	flow coefficient
η	vertical axis of transformed coordinate
$\hat{\delta}^+, \bar{\delta}^+$	limited slopes
A	Jacobian matrix for $\overline{\mathbf{E}}$
$\mathbf{A}^{\pm}$	decomposed matrix of **A**
$\mathbf{A}_v$	Jacobian matrix for $\overline{\mathbf{E}}_v$
B	Jacobian matrix for $\overline{\mathbf{F}}$
$\mathbf{B}_v$	Jacobian matrix for $\overline{\mathbf{F}}_v$
c	velocity of sound
E	total energy vector
$\overline{\mathbf{E}}$	transformed unknown vector
$\overline{\mathbf{E}}_v$	transformed unknown vector
F	flux vector
$\mathbf{F}_E$	inviscid flux vector
$\mathbf{F}_v$	inviscid flux vector
$\overline{\mathbf{F}}$	transformed unknown
$\overline{\mathbf{F}}_v$	transformed unknown vector
g(**A**)	any matrix having the right and left eigenvectors
H	total enthalpy
I	unit tensor
i	cell index in ξ direction iblock block index
imax	maximum cell index in ξ direction
j	cell index in η direction
J	Jacobian of transformation
Jmax	maximum cell index in η direction
k	$k = \frac{C_p}{C_v}$
ℓ	limiter function
L	eigenvector matrix of **A**
$\mathbf{L}^{-1}$	Inverse matrix of **L**
M	Mach number
M_{in}	inlet Mach number
N	normal vector of **A**
P	thermodynamic pressure
P_s	static pressure
P_t	total pressure
Pin	inlet pressure
q	heat flux
Q	vector of consevative variables
$\overline{\mathbf{Q}}$	transformed vector of consevative variables
R	Reaction factor
R	parameter of MUSCL limiter
Re_η	minimum cell Reynolds number in η direction
Re_ξ	minimum cell Reynolds umber in ξ directon
Re_c	minimum cell Reynolds number
r_h	hub radius
r_t	tip radius
S_f	safety factor for time step
t	time in physical coordinate
T_s	static temperature
T_s	static temperature
T_t	total temperature
Tin	inlet temperature
u	velocity vector
u	x-direction velocity component
U	contravariant velocity in ξ direction

$\tilde{u}$	averaged u at cell boundary
V	contravariant velocity in η direction
v	y-direction velocity component
V_{in}	relative inlet velocity
V	volume
x	vertical axis of Cartesian coordinate
x_ξ	partial of x with respect to ξ
x_η	partial of x with respect to η
y	horizontal axis of Cartesian coordinate
y_ξ	partial of y with respect to ξ
y_η	partial of y with respect to η

Subscript

ξ	partial derivative with respect to ξ
η	partial derivative with respect to η
b	index of bottom face flux
h	hub for blade radius
E	inviscid flux vector
I	mesh point index in ξ direction
in	inlet condition
j	mesh point index in η direction
l	index of left face flux
r	index of right face flux
s	static thermodynamic properties
t	index of top face flux
t	tip for blade radius
t	total state for thermodynamic properties
x	partial derivity with respect to x
y	partial derivity with respect to y
v	viscous flux vector

Superscript

+	positive split flux
–	negative split flux
n	previous time level
n+1	current time level
T	transpose of matrix

REFERENCES

1. Inue, M., Kuroumaru, M., Tanino, T. and Furukawa, M., "Propagation of Multiple Short-Length-Scale Stall Cells in an Axial Compressor Rotor", ***ASME Journal of Turbomachinery***, Vol. 122, (2000), 45-53.
2. Day, I. J., Breuer, T., Escuret, J., Cherrett, M. and Wilson, A., "Stall Inception and the Prospects for Active Control in Four High-Speed Compressors", ***ASME Journal of Turbomachinery***, Vol. 121, (1999), 18-27.
3. Silowski, P. D., "Measurements of Rotor Stalling in a Matched and a Mismatched Multistage Compressor", ***GTL Report, Gas Turbine Laboratory, Massachusetts Institute of Technology***, No. 221, (1995).
4. Garnier, V. H., Epstein, A. H. and Greitzer, E. M., "Rotating Waves as a Stall Inception Indication in Axial Compressors", ***ASME Journal of Turbomachinery***, Vol. 113, (1991), 290-301.
5. Moore, F. K. and Greitzer, E. M., "A Theory of Post-Stall Transients in Axial Compression System: Part I, II", ***ASME Journal of Engineering for Gas Turbines and Power***, Vol. 108, (1986), 68-76 and 231-239.
6. Longley, J. P., "A Review of Nonsteady Flow Models for Compressors Stability", ***ASME Journal of Turbomachinery***, Vol. 116, (1994), 202-215.
7. Hendricks, G. J., Sabnis, J. S. and Feulner, M. R., "Analysis of Instability Inception in High-Speed Multistage Axial Flow Compressors", ***ASME Journal of Turbomachinery***, Vol. 119, (1997), 714-722.
8. He, L., "Computational Study of Rotating-Stall Inception in Axial Compressors," ***AIAA Journal of Propulsion and Power***, Vol. 13, No. 1, (1997), 31-38.
9. Nishizawa, T. and Takata, h., "Numerical Study on Rotating Stall in Finite Pitch Cascades", ASME Paper No. 94-GT-258, (1994).
10. Outa, E., Kato, D. and Chiba, K., "A N-S Simulation of Stall Cell Behavior in a 2-D Compressor Rotor-Stator System at Various Load", ASME Paper No. 94-GT-257, (1994).
11. Saxer-Flelici, H. M., Saxer, A. P., Inderbitzen, A., Gyarmathy, G., "Prediction and Measurement of Rotating Stall Cell in an Axial Compressor", ***ASME Journal of Turbomachinery***, Vol. 121, (1999), 365-375.
12. Hoffman, K. A. and Chiang, S. T., "Computational Fluid Dynamics for Engineers", A Publication of Engineering Education System™, Wichita, Kansas, 67208-1078, USA, ISBN 0-9623731-7-6, (1993).
13. Peyret, R., Grasso, F. and Meola, C., "Handbook of Computational Fluid Mechanics; Chapter No. 4: Euler and Navier-Stokes Equations for Compressible Flows: Finite Volume Methods", Academic Press, ISBN 0-12-553010, (1996).
14. Bohn, D. and Emunds, R., "A Navier-Stokes Computer Code for Theoretical Investigations on the Application of Various Turbulence Models for Flow Prediction Along Turbine Blades", ***Proceeding of the International Gas Turbine and Aero-Engine Congress and Exposition***, Houston, Texas-June 5-8, 95-GT-90, (1995).
15. Granville, P. S., "Baldwin-Lomax Factors for Turbulent Boundary Layers in Pressure Gradients", ***AIAA Journal***, 25, (12), (1987).

16. He, L., "Computational Study of Rotating-Stall Inception in Axial Compressors", ***Journal of Propulsion and Power***, 13, (1), (January-February, 1997), 31-38.
17. Hirsch, Ch., "*Numerical Computation of Internal and External Flows, Volume 1: Fundamentals of Numerical Discretization*", A Wiley-Interscience Publication, ISBN 0 471 917621, (1988).
18. Sanz, W. and Platzer, M., F., "On the Navier-Stokes Calculation of Separation Bubbles with a New Transition Model", Presented at the ***International Gas Turbine and Aero-Engine Conference and Exhibition***, Birmingham, UK-June 10-13, 96-GT-487, (1996).
19. Fletcher, C. A. J., "Computational Techniques for Fluid Dynamics 2: Springer-Verlag, ISBN 0-387-18759-6, (1991).